Journal of Non-Crystalline Solids 356 (2010) 2965–2968

Thermal stability of glasses from the $Fe_4(P_2O_7)_3$–$Fe(PO_3)_3$ system

Liying Zhang [a], Luciana Ghussn [b], Melodie L. Schmitt [a], Edgar D. Zanotto [b], Richard K. Brow [a,*], Mark E. Schlesinger [a]

[a] Department of Materials Science and Engineering, Missouri University of Science and Technology, Rolla, MO, USA
[b] Department of Materials Engineering, Federal University of São Carlos, São Carlos, Brazil

ARTICLE INFO

Article history:
Received 15 October 2009
Received in revised form 22 March 2010
Available online 24 August 2010

Keywords:
Iron phosphate glass;
Ferric pyrophosphate;
Ferric metaphosphate;
Glass stability

ABSTRACT

Iron phosphate glasses with nominal Fe/P compositions between 0.50 and 0.67 were prepared and characterized. The effects of melt conditions and the initial composition on the Fe(II)-content are reported. Characteristic temperatures, including the glass transition temperature and crystallization temperature, were measured by DSC. The stability of melts against crystallization, described by the Angel and Weinberg parameters, generally decreases with increasing O/P and Fe/P ratios.

1. Introduction

Iron phosphate glasses and crystals have interesting chemical, thermal and electrical properties. Crystalline iron phosphate compounds have been developed for several applications, including catalysts, optical materials and electrodes [1–5]. Chemically durable iron phosphate glasses have been studied as alternative materials for vitrifying high-level nuclear waste [6–10]. Other iron phosphate glasses have been developed for corrosion-resistant, reinforcing fibers for composite materials [11,12].

The *liquidus* behavior of a melt can provide information useful for making glasses. Wentrup reported a portion of the phase diagram for the Fe_2O_3–$Fe_4(P_2O_7)_3$ system [13], but did not cover the conventional glass-forming range for iron phosphate compositions, where the nominal Fe_2O_3/P_2O_5 molar ratio is between 1/3 and 2/3 [2–4,14–16]. More recently, we have reported the ferric phosphate *liquidus* surface between $Fe(PO_3)_3$ and Fe_3PO_7 [17], updating and expanding Wentrup's analysis. In that study, we report the presence of a eutectic point between $Fe(PO_3)_3$ and $Fe_4(P_2O_7)_3$ at 37.0 mol% Fe_2O_3 and 907 °C. This point is near the baseline compositions of glasses developed for vitrifying nuclear wastes.

Angell and other researchers suggested that the difference between the glass transition temperature (T_g) and the crystallization peak temperature (T_p) from a DTA experiment, $K_A = (T_p - T_g)$, is a measure of the stability of a supercooled glass melt against crystallization: the greater the value of K_A, the more stable the melt is against crystallization [18,19]. Weinberg used the parameter $(T_p - T_g)/T_m$, where T_m is the melting temperature, to describe the stability of supercooled melts that crystallize congruently [20]. As reported by Nascimento et al. [21], a modified form of the Weinberg parameter, $K_W = (T_X - T_g)/T_L$, where T_X is the crystallization onset temperature and T_L is the *liquidus* temperature, can be used to describe the stability of melts against crystallization.

Information about the thermal stability of supercooled iron phosphate glasses against crystallization is quite useful for the consideration of these glasses as hosts for nuclear wastes and for other applications, such as processing glass fibers which should not devitrify on the cooling path during fabrication. In the present work, the modified Weinberg parameter (K_W) and the Angell parameter ($K_A = T_X - T_g$) are used to describe the stability against crystallization of iron phosphate melts.

2. Experimental procedures

From 60 to 100 g of glass with nominal compositions between 33 and 40 mol% Fe_2O_3 were melted in alumina crucibles in air for 2 h either at 1100 °C or 1200 °C. Fe_2O_3 and $NH_4H_2PO_4$ were used as the raw materials. Prior to melting, the batches were calcined at 500 °C for 4 h to remove ammonia and water. Melts were quenched on steel plates to form glasses. Powders (≤53 μm) were obtained by grinding the quenched glass in a mortar with a pestle. These powders were analyzed by differential scanning calorimetry (Netzsch 404), using alumina sample pans in air at a heating rate of 10 °C/min. Samples were analyzed by X-ray diffraction (Scintag XDS 2000) and Raman spectrometry (Horiba–Jobin Yvon LabRam-HR); the latter used a He–Ne laser (632.8 nm) as the excitation source. The Fe(II) content of the glasses was determined by titration using a 2 mM $KMnO_4$ solution [22].

* Corresponding author. Tel.: +1 573 341 6812; fax: +1 573 341 2071.
E-mail address: brow@mst.edu (R.K. Brow).

0022-3093/$ – see front matter © 2010 Elsevier B.V. All rights reserved.
doi:10.1016/j.jnoncrysol.2010.03.044

Glass powders were crystallized by heating at temperatures between 600 and 850 °C for 12 h and the detected phases were prepared and studied by DTA/TGA (Netzsch STA 409C) to help interpret the DSC data obtained from the glasses. $FePO_4$ was prepared by dehydrating $FePO_4 \cdot xH_2O$ (100%, Alfa Aesar). $Fe(PO_3)_3$ was prepared by heating a stoichiometric mixture of $FePO_4$ and $NH_4H_2PO_4$ (98%, Alfa Aesar), first for 6 h at 500 °C for calcination, then for 12 h at 800 °C. $Fe_4(P_2O_7)_3$ was made by the solid state reaction of $FePO_4$ and $Fe(PO_3)_3$ at 800 °C for 12 h and then at 940 °C for 12 h [23]. $Fe_3(P_2O_7)_2$ was prepared by heating a stoichiometric mixture of $Fe(PO_3)_3$ and Fe_2PO_5 in a sealed ampule at 900 °C for 12 h. Fe_2PO_5 was prepared according to the method described by Modaressi, et al. [24]. The purity of these crystallized samples was confirmed by X-ray diffraction.

3. Results

3.1. Redox ratio and Raman spectra

Fig. 1 shows the measured Fe(II) contents and the calculated O/P ratios of glasses with different nominal Fe/P ratios, quenched from melts held in air for 2 h at different temperatures. Glasses with the same nominal Fe/P ratio quenched from melts held at 1200 °C have greater Fe(II) contents than glasses melted at 1100 °C, and the loss of oxygen associated with the reduction of Fe(III) to Fe(II) reduces the nominal O/P ratio. In addition, glasses with greater nominal Fe/P ratios have greater fractions of Fe(II), when melted under the same conditions. These results are similar to those reported for the effects of melt history on the composition and structure of 40.0 mol% Fe_2O_3 glasses [25]. The redox behavior of iron phosphate melts will be described in another publication [26]. The uncertainty in the Fe(II)-contents shown in Fig. 1 represents the standard deviations from three titrations for each sample.

Based on the analyzed Fe(II) contents, the glass compositions can be relocated in the ternary ferrous–ferric phosphate compositional diagram (Fig. 2), where it is seen that these glasses have compositions that fall between the metaphosphate and pyrophosphate stoichiometries (dashed lines). The region outlined by the solid lines represents the glass compositions reported in the literature [25,26], and the glasses studied here generally fall in the same region.

Raman spectra of the glasses melted at 1100 °C are shown in Fig. 3. Broad peaks or shoulders in the 1000–1200 cm^{-1} range are assigned to the symmetric and asymmetric stretching modes of nonbridging oxygens on Q^1 and Q^2 tetrahedra [27,28]. (The superscript 'x' in the Q^x notation refers to the number of bridging oxygens per P-tetrahedron.)

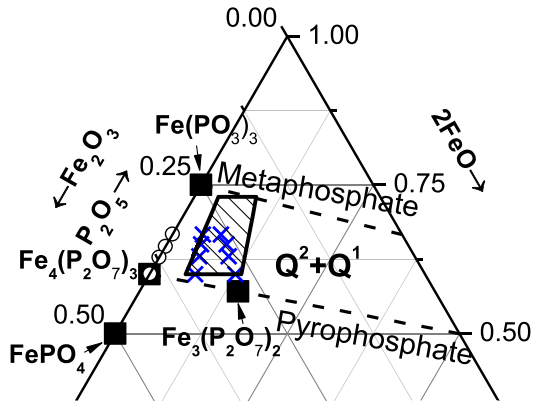

Fig. 2. Compositions of glasses prepared in this study. ○ — nominal composition of the batch; × — analyzed glass compositions; ■ — crystalline phases identified in partially-crystallized samples.

The broad peaks between 600 and 800 cm^{-1} are assigned to the symmetric stretching modes of P–O–P bonds that link neighboring P-tetrahedra [29]. For glasses with increasing nominal iron content, the relative fraction of Q^1 units is expected to increase, consistent with the shift in the P–O stretching mode from 1069 to 1037 cm^{-1} as the O/P ratio increases from 3.22 to 3.44. The relative intensity of the peak due to the P–O–P stretching mode (near 700 cm^{-1}) also decreases with increasing O/P ratio. The spectral trends for the glasses melted at 1200 °C (not shown) are similar.

3.2. Crystallization behavior

Fig. 4 shows DSC patterns collected in air for the glasses melted at 1100 °C and 1200 °C. At least two exothermic peaks are detected when each sample is heated. For glasses with increasing iron contents melted at a constant temperature, T_g decreases slightly and T_X is largely unchanged.

Marasinghe reported similar DTA patterns for the glasses with batch compositions near 40.0 mol% Fe_2O_3, and reported that the first exothermic peak ~640 °C is due to the crystallization of $Fe_3(P_2O_7)_2$, which mostly (90%) transforms to $Fe_4(P_2O_7)_3$ at ~800 °C [30]. In this work, three crystalline phases, $FePO_4$, $Fe_3(P_2O_7)_2$ and $Fe_4(P_2O_7)_3$, were detected in the heat-treated samples. The thermal behavior of the crystalline phases formed in the glasses can help explain the endothermic events around 900 °C in the patterns in Fig. 4 as shown below.

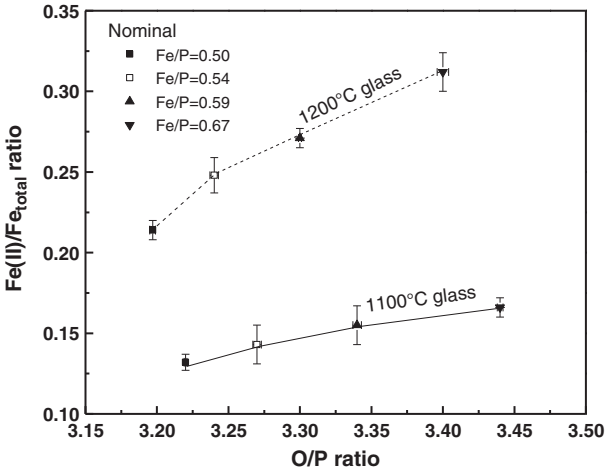

Fig. 1. Redox ratio and O/P ratio of glasses with different nominal Fe/P ratios melted in air for 2 h at different temperatures. The lines are guides for the eye.

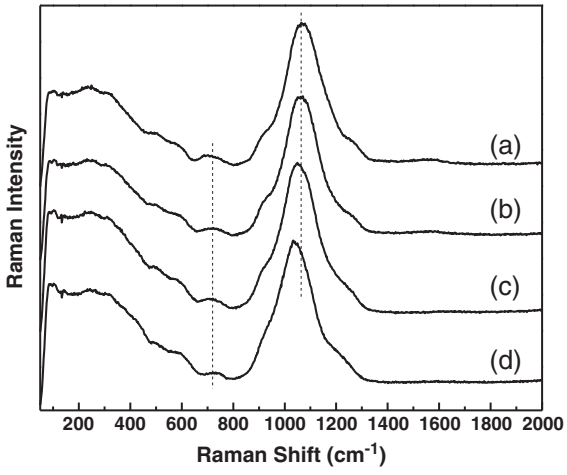

Fig. 3. Raman spectra of glasses melted at 1100 °C with a nominal Fe_2O_3 content of (a) 33.3 mol%; (b) 35.4 mol%; (c) 37.2 mol%; and (d) 40.0 mol%.

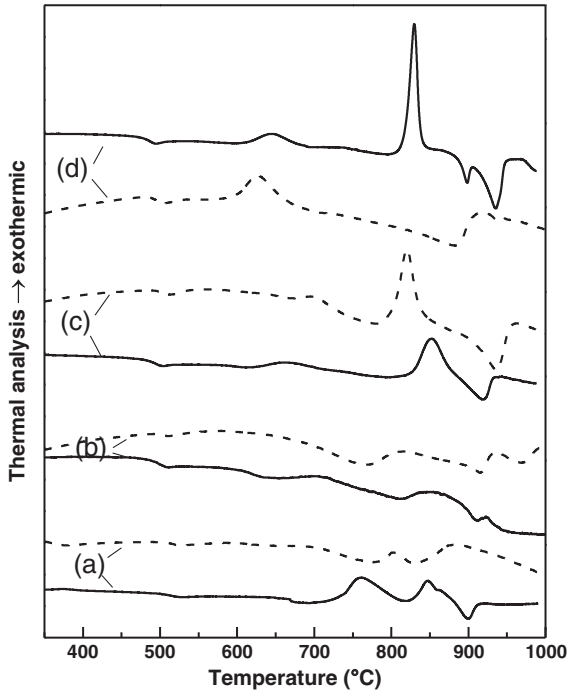

Fig. 4. DSC patterns for 1100 and 1200 °C series of glasses as solid and dashed lines, respectively, with nominal Fe_2O_3 of (a) 33.3 mol%; (b) 35.4 mol%; (c) 37.2 mol%; and (d) 40.0 mol%.

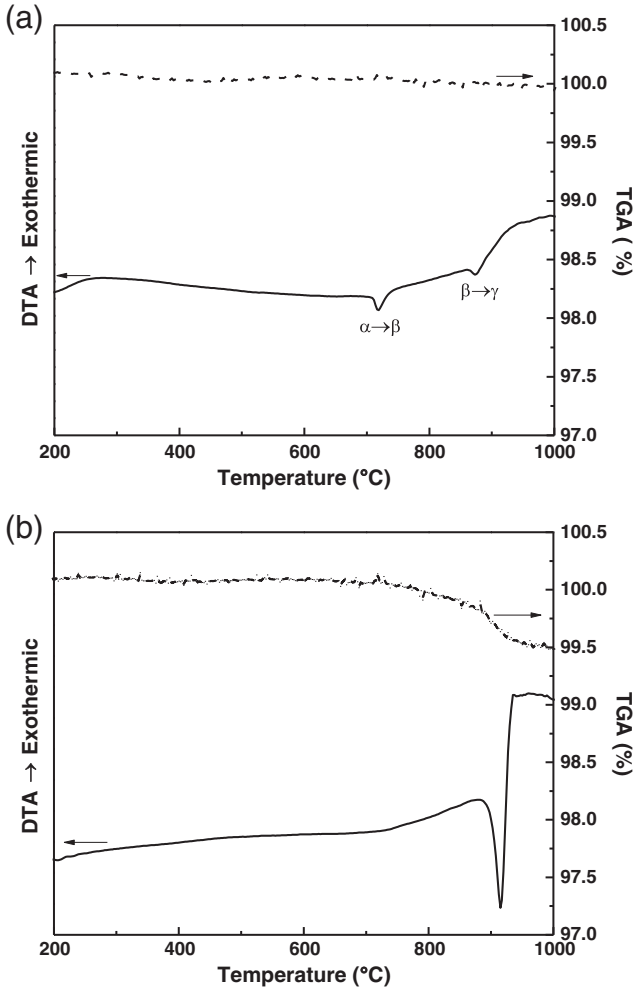

Fig. 5. DTA/TGA patterns of (a) $FePO_4$ and (b) $Fe_4(P_2O_7)_3$ crystals heated in air.

Fig. 5 shows DTA/TGA data collected in air from crystalline $FePO_4$ and $Fe_4(P_2O_7)_3$ powders. $FePO_4$ is stable below 1000 °C, exhibiting two endotherms related to solid phase transitions [13,31]. In contrast, $Fe_4(P_2O_7)_3$ loses some weight above 800 °C because of the reduction of Fe(III) to Fe(II). The slope of the DTA baseline changes around 900 °C because of the change in heat capacity when the solid melts. $Fe_3(P_2O_7)_2$ decomposes around 925 °C [32]. The reported thermal behavior of the compounds indicates that the endothermic events around 900 °C in the DSC patterns of the glass (Fig. 4) are related to the melting and decomposition of $Fe_4(P_2O_7)_3$ and $Fe_3(P_2O_7)_2$.

Table 1 lists the values of T_g and the onset temperature of the first crystallization peak, T_X, obtained from the DSC scans for each glass. The uncertainty in T_g and T_X was estimated to be ±5 °C, based on multiple runs for the glasses studied in this work. Also listed are the estimated ranges of liquidus temperatures (from [17]), and the values for K_A and K_W for the two series of glasses.

4. Discussion

The glass transition temperature decreases with increasing nominal Fe_2O_3 content (Table 1). There are two structural effects caused by iron oxide additions: a decrease in the relative fraction of oxygens that bridge neighboring P-tetrahedra and an increase in the number of oxygens that link neighboring Fe-polyhedra with the P-tetrahedra. The increase in the O/P ratios for the glasses with increasing Fe_2O_3-content (Table 1) indicates that the number of P–O–Fe bonds increases relative to the number of P–O–P bonds.

Glass stability is evaluated using the characteristic temperatures collected by DTA and other techniques [17], using the Angell parameter K_A and Weinberg parameter K_W. Fig. 6 shows the dependence of the glass stability parameters on glass composition. The trends in K_A and K_W both indicate that supercooled melts with lower O/P and lower Fe/P ratios have greater stability against crystallization. These results indicate that melts which possess longer P–O–P chains are more difficult to crystallize, which is also consistent with laboratory experience. There is little discernible effect of Fe(II) content on glass thermal stabilities.

Table 1
The summary of T_L and DTA/DSC characteristic parameters.

Nominal Fe_2O_3 mol%	1100 °C series						1200 °C series					
	O/P	T_L range[a]	T_g (°C)	T_X (°C)	K_A (°C)	K_W[b]	O/P	T_L range[a]	T_g (°C)	T_X (°C)	K_A (°C)	K_W[b]
33.3	3.22	1030–1060	500	728	228	0.171–0.175	3.20	1025–1065	506	785	279	0.209–0.215
35.4	3.27	990–1010	485	646	161	0.125–0.127	3.24	985–1015	493	767	274	0.213–0.218
37.2	3.34	880–910	482	616	134	0.113–0.116	3.30	875–915	493	671	178	0.150–0.155
40	3.44	920–950	476	606	130	0.106–0.109	3.40	915–955	484	597	113	0.092–0.095

[a] *Liquidus* temperatures are given as a range, based on reported data in [17] and laboratory experience.
[b] Errors are from the *liquidus* temperature range.

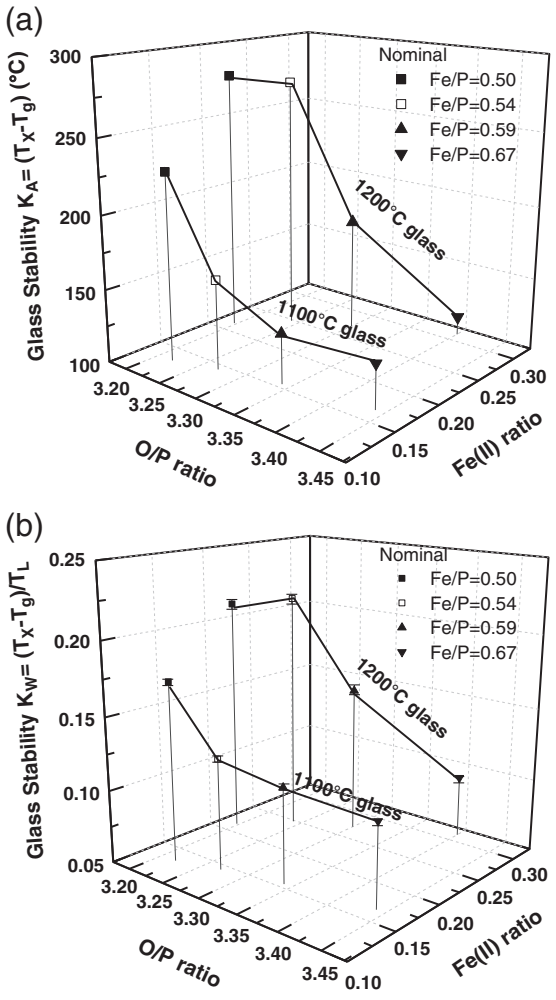

Fig. 6. Glass stability parameters (a) K_A and (b) K_W for iron phosphate glasses as functions of the O/P, Fe/P and Fe(II) content. The lines are guides for the eye.

5. Summary

The characteristic temperatures of melted from compositions in the $Fe_4(P_2O_7)_3$–$Fe(PO_3)_3$ system were determined and used to evaluate the stability of melts against crystallization. It was found that decreases in the nominal Fe/P and O/P ratios yield supercooled melts that are more stable against crystallization. This information is useful for the design of good glass-forming compositions.

Acknowledgements

The authors gratefully acknowledge Jong Wook Lim for his kind assistance in the collection of the Raman spectra. This material is based upon work supported by the National Science Foundation (U.S.A.) under Grants No. DMR-0305202 and DMR-0502463, by CNPq (Brazil) Grant no. 492565/04-0 and by FAPESP (Brazil) Grant 07/08179-9.

References

[1] R.C. Haushalter, L.A. Mundi, Chem. Mater. 4 (1992) 31.
[2] A. Clearfield, Chem. Rev. 88 (1988) 125.
[3] K. Zaghib, C.M. Julien, J. Power Sources 142 (2005) 279.
[4] M. Ai, K. Ohdan, Appl. Catal. A 180 (1999) 47.
[5] N. Aliouane, T. Badechet, Y. Gagou, E. Nigrelli, P. Saint-Gregoire, Ferroelectrics 241 (2000) 255.
[6] X. Yu, D.E. Day, G.J. Long, R.K. Brow, J. Non-Cryst. Solids 215 (1997) 21.
[7] W. Huang, D.E. Day, C.S. ray, C.W. Kim, J. Nucl. Mater. 346 (2005) 298.
[8] X. Fang, C.S. Ray, G.K. Marasinghe, D.E. Day, J. Non-Cryst. Solids 263 and 264 (2000) 293.
[9] L. Kahl, D. Clark, W. White, Adv. Ceram. 20 (1986) 141.
[10] B. Samuneva, P. Tzvetkova, I. Gugov, V. Dimitrov, J. Mater. Sci. Lett. 15 (1996) 2180.
[11] V. Simon, S.G. Chiuzbăian, M. Neumann, D. Eniu, E. Indrea, A. Tőrők-kiss, S. Simon, Mod. Phys. Lett. B 14 (2000) 767.
[12] S.T. Lin, S.L Krebs, S. Kadiyala, K.W. Leong, W.C. LaCourse, B. Kumar, Biomaterials 15 (1994) 1057.
[13] H. Wentrup, Arch. Eisenhüt. 9 (7) (1935) 57.
[14] Y.M. Moustafa, K. El-Egili, H. Doweidar, I. Abbas, Phys. B 353 (2004) 82.
[15] M. Karabulut, M. Yuksek, G.K. Marasinghe, D.E. Day, J. Non-Cryst. Solids 355 (2009) 1571.
[16] D.E. Day, Z. Wu, C.S. Ray, P. Hrma, J. Non-Cryst. Solids 241 (1998) 1.
[17] L. Zhang, M.E Schlesinger, R.K. Brow, J. Am. Ceram. Soc. submitted.
[18] E.I. Cooper, C.A. Angell, J. Non-Cryst. Solids 56 (1983) 75.
[19] M.G. Drexhage, O.H. El-Bayoumi, H. Lipson, S.T. Moynihan, A.J. Bruce, J. Lucas, G. Fonteneau, J. Non-Cryst. Solids 56 (1983) 51.
[20] M.C. Weinberg, Phys. Chem. Glasses 35 (1994) 119.
[21] M.L.F. Nascimento, L.A. Souza, E.B. Ferreira, E.D. Zanotto, J. Non-Cryst. Solids 351 (2005) 3296.
[22] S.I. Grishin, J.M. Bigham, O.H. Tuovinen, Appl. Environ. Microbiol. 54 (1988) 3101.
[23] C. Gleitzer, Eur. J. Solid State Inorg. Chem. 28 (1991) 77–91.
[24] A. Modaressi, A. Courtois, R. Gerardin, B. Malaman, C. Gleitzer, J. Solid State Chem. 40 (1981) 301.
[25] X. Fang, C.S. Ray, A. Mogus-Milankovic, D.E. Day, J. Non-Cryst. Solids 283 (2001) 162.
[26] M.L. Schmitt, R.K. Brow, M.E. Schlesinger, "Predicting the Iron Redox Ratio in Iron Phosphate Melts: A Thermodynamic Model," to be submitted.
[27] A. Mogus-Milankovic, B. Pivac, K. Furic, D.E. Day, Phys. Chem. Glasses 38 (1997) 74.
[28] C. Nelson, D.R. Tallant, Phys. Chem. Glasses 26 (1985) 119.
[29] A.M. Efimov, J. Non-Cryst. Solids 209 (1997) 209.
[30] G.K. Marasinghe, M. Karabulut, C.S. Ray, D.E. Day, M.G. Shumsky, W.B. Yelon, C.H. Booth, P.G. Allen, D.K. Shuh, J. Non-Cryst. Solids 222 (1997) 144.
[31] E.C. Shafer, M.W. Shafer, R. Roy, Z. Krist. 108 (1956) 263.
[32] L. Zhang, Phase Equilibria in the Iron Phosphate System, Ph.D. dissertation, Missouri University of Science and Technology (2010).